Interplay between Confinement and Drag Forces Determine the Fate of Amyloid Fibrils

Kathleen Beth Smith,[1] Monika Wehrli,[1] Aleksandre Japaridze,[2] Salvatore Assenza,[1,†] Cees Dekker,[2] and Raffaele Mezzenga[1,3,*]

[1]Department of Health Sciences and Technology, Swiss Federal Institute of Technology in Zurich, 8092 Zurich, Switzerland
[2]Department of Bionanoscience, Kavli Institute of Nanoscience Delft, Delft University of Technology, Van der Maasweg 9, 2629 HZ, Delft, Netherlands
[3]Department of Materials, Swiss Federal Institute of Technology, Zurich, 8093, Zurich, Switzerland

(Received 8 July 2019; accepted 26 February 2020; published 19 March 2020)

The fine interplay between the simultaneous stretching and confinement of amyloid fibrils is probed by combining a microcapillary setup with atomic force microscopy. Single-molecule statistics reveal how the stretching of fibrils changed from force to confinement dominated at different length scales. System order, however, is solely ruled by confinement. Coarse-grained simulations support the results and display the potential to tailor system properties by tuning the two effects. These findings may further help shed light on *in vivo* amyloid fibril growth and transport in highly confined environments such as blood vessels.

DOI: 10.1103/PhysRevLett.124.118102

Amyloid fibrils are biopolymers often associated with neurodegenerative diseases [1,2], though functional amyloid fibrils have also been reported *in vivo* [3,4], where, for example, they assist blood coagulation [5]. *In vitro*, their formation has been correlated with extreme shear and confinement [6–8]. *In vivo*, this could be analogous to the biological conditions proteins are submitted to, such as $A\beta$ proteins in the brain parenchyma and narrow brain perivascular pathways [9]. The aggregation into plaque and even degradation of fully formed fibrils has also been linked to such conditions [6–8]. It is therefore important to investigate how biopolymers, and specifically amyloid fibrils, react to stress, strain, and confinement [10–12].

To this effect, polymer physics has great potential, as polymer chains under a force [13–15] or confinement [13,16] have been extensively studied both theoretically and experimentally. Initially, studies were carried out using fluorescence microscopy [17–19]. However, by taking setups applicable to atomic force microscopy (AFM), it is possible to obtain higher resolution images of polymers under confinement [20,21] or extension [22], thus leading to detailed statistical characterization at the single-molecule level.

It is well accepted that both a pulling force and confinement contribute to the extension and alignment of polymers. However, combining the two has proven to be an outstanding problem in polymer physics, and only recently, theoretical and numerical contributions have emerged extending the Odijk deflection length [16] to include a force-extension relation [23,24]. To our knowledge there are no extensions to the de Gennes regime [13] and no experimental studies examining the properties of polymers emerging from the simultaneous contribution of these two effects. In this Letter, we carried out a detailed study on the behavior of biopolymers subjected to both an external force and spatial confinement by employing beta-lactoglobulin (BLG) amyloid fibrils as a model system [25–28]. We achieved this by using a microcapillary setup compatible with AFM, previously described [20] and depicted in Fig. 1 [29]. The microfabrication of this setup let us control the polydimethylsiloxane (PDMS) slit size, and therefore the confinement of the system, with submicron precision. The capillary force f in a rectangular channel of width W (and constant height H) follows the proportionality [31]

$$f \propto W \cos\theta_e, \tag{1}$$

with θ_e the contact angle of the amyloid solution with the surface of the microcapillary. This capillary force is the driving effect in the capillary action. Therefore, changing the capillary force has a direct impact on the viscous drag forces applied to the fibrils. Hence, for a larger width W, i.e., larger capillary force and subsequent drag forces [see Sec. S2.1 in Supplemental Material (SM) [29]], the fibrils are subject to a higher force, despite being subject to a lower degree of confinement. Thanks to the nanometer resolution of the AFM and resulting quality of the statistical analysis, the subtle interplay between confinement and pulling force could be observed by tuning the width of the microcapillaries.

In order to minimize the cross-variation between samples, the following points were attended to. First, as depicted in Figs. 1(b) and 1(c), the PDMS slits are placed on a mica surface. Once the fibrils solution has been deposited, the PDMS slits are removed, and the fibrils adsorbed to the mica surface are imaged, Fig. 1(d). This mica is freshly cleaved, with no plasma treatment, unlike the PDMS sides of the channel; therefore, the adsorption

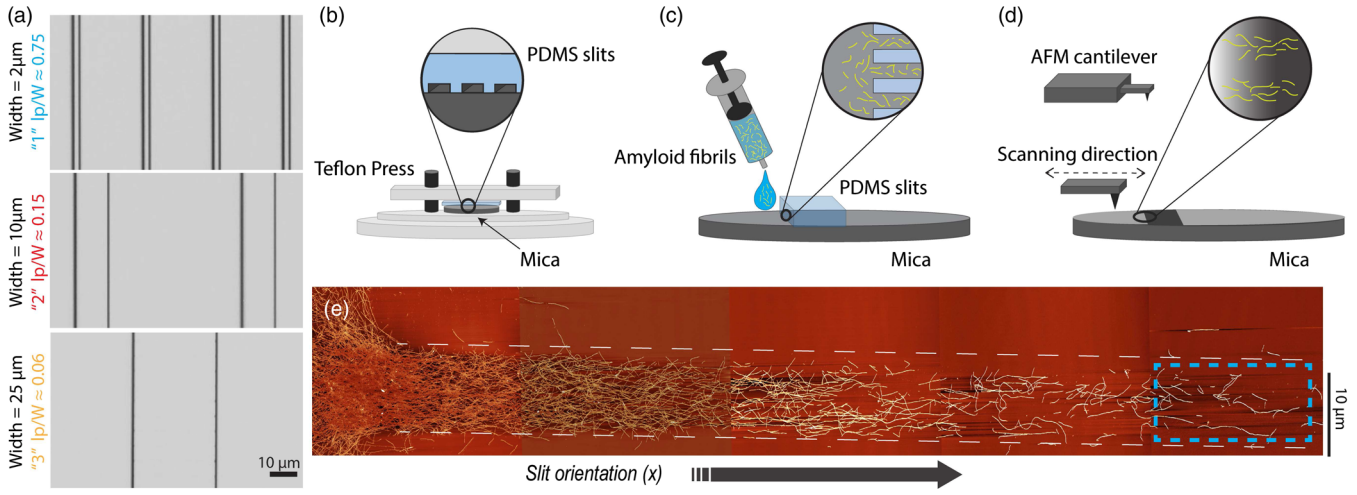

FIG. 1. (a) Light microscopy images of etched silicon wafers used for the replica molding of PDMS slits. Height of the patterns is constant at 2.1 μm. (b) After plasma treatment, the PDMS slits are placed on freshly cleaved mica and gently clamped in a Teflon press. (c) A 0.0001 wt % solution of dialyzed BLG amyloid fibrils is deposited to one side of the slits, and the whole sample placed in a warm humid environment for 30 min to allow time for the fibrils to migrate into the slits and equilibrate. (d) The sample is gently rinsed, the clamp and slits removed, rinsed again, and dried with pressurized air, to then be imaged with AFM. (e) Typical resulting AFM images of the sample preparation described in (b)–(d) using slit "2" of 10 μm ($l_p/W \approx 0.15$). The dashed blue box represents the concentration of fibrils considered for statistical analysis and x denotes the direction of the slits. Scale bar is 10 μm.

process is the same for every experiment. Second, in Fig. 1(e) we observe a gradient in concentration along the axis of the slit. To keep the contribution due to mutual repulsion among fibrils to a minimum, only the fibrils deepest in the slits and at lower concentrations were analyzed [see Fig. 1(e) and Figs. S1 and S2 of SM [29] for typical images and fibril concentrations]. Third, from previous work [28], it is known that different populations of BLG fibrils coexist, characterized by specific values of height and corresponding persistence length l_p. Therefore, to exclude any bias due to sample heterogeneity, we characterized the fibrils present inside the slits by measuring their average height; see Sec. S2.2 and Fig. S3 of SM [29]. Only the population of fibrils having a height of about 4 nm, corresponding to a $l_p \approx 1500$ nm [28], was present in the slits, independent of W. We could therefore characterize the different levels of confinements by the ratios l_p/W, as is commonly used in the literature [13,16]. Lastly, we carried out a control experiment, in order to determine whether the capillary force was contributing to the observed results. Keeping the width of the channel constant, the capillary force was increased by changing the plasma treatment time and thus decreasing the θ_e of the PDMS microcapillaries [32]. An increase in fibril orientation and stretching was observed (see Sec. S2.2 of SM [29]), indicating that the system can indeed capture the action of the force. To summarize, our controls confirm that all the results displayed in the following can be attributed to the effect of confinement and force.

Experiments were carried out in capillaries of three different widths, Fig. 1(a). For visualization purposes, the ratios of $l_p/W \approx 0.75$, 0.15, 0.06 were assigned numbers from 1 to 3 as a function of the increase in width and subsequently force. Indeed, the channels were each exposed to a plasma time of 10 s, θ_e was therefore a constant, and Eq. (1) becomes $f \propto W$. Figure 2(a) shows the mean-square end-to-end distance $\langle R^2(l)\rangle$ as a function of internal contour length l for fibrils present in these different slits. From the enlargement at shorter contour lengths we observe a regime dominated by the force, where the relative order of the curves follows the increase in force, as displayed by the sequence 1-2-3 (read from the bottom up). However, at larger contour lengths, we observe a shift in regime for the slit "1"; the trend then becomes 2-1-3. This change in regime can be understood when we consider that shorter fibers or segments are less sensitive to the confinement due to their smaller radius of gyration [13,16]; thus at small l the force dominates the trend. However, once a certain length is reached, the fibrils are affected by the confinement, which becomes more prominent than the action of the force. This leads to the inversion observed, where $\langle R^2(l)\rangle_1$ overtakes $\langle R^2(l)\rangle_2$.

To quantify this effect, Fig. 2(b) shows the decay of the scaling exponent $\nu(l)$ [13,33], extracted from the values in Fig. 2(a) by assuming $\langle R^2(l)\rangle \sim l^{2\nu(l)}$. Additionally, in the inset we report $\Delta_{12} = (d/dl)\langle R^2(l)\rangle_1 - (d/dl)\langle R^2(l)\rangle_2$, the difference in slopes of the end-to-end distance of slits "1" and "2." This inset clearly shows the transition from one effect to the other. The force initially dominates; hence Δ_{12} is negative and decreasing. At such short scales, one expects the leading order to be $\langle R(l)^2\rangle \approx l^2$, as confirmed by the linear behavior of the individual derivatives

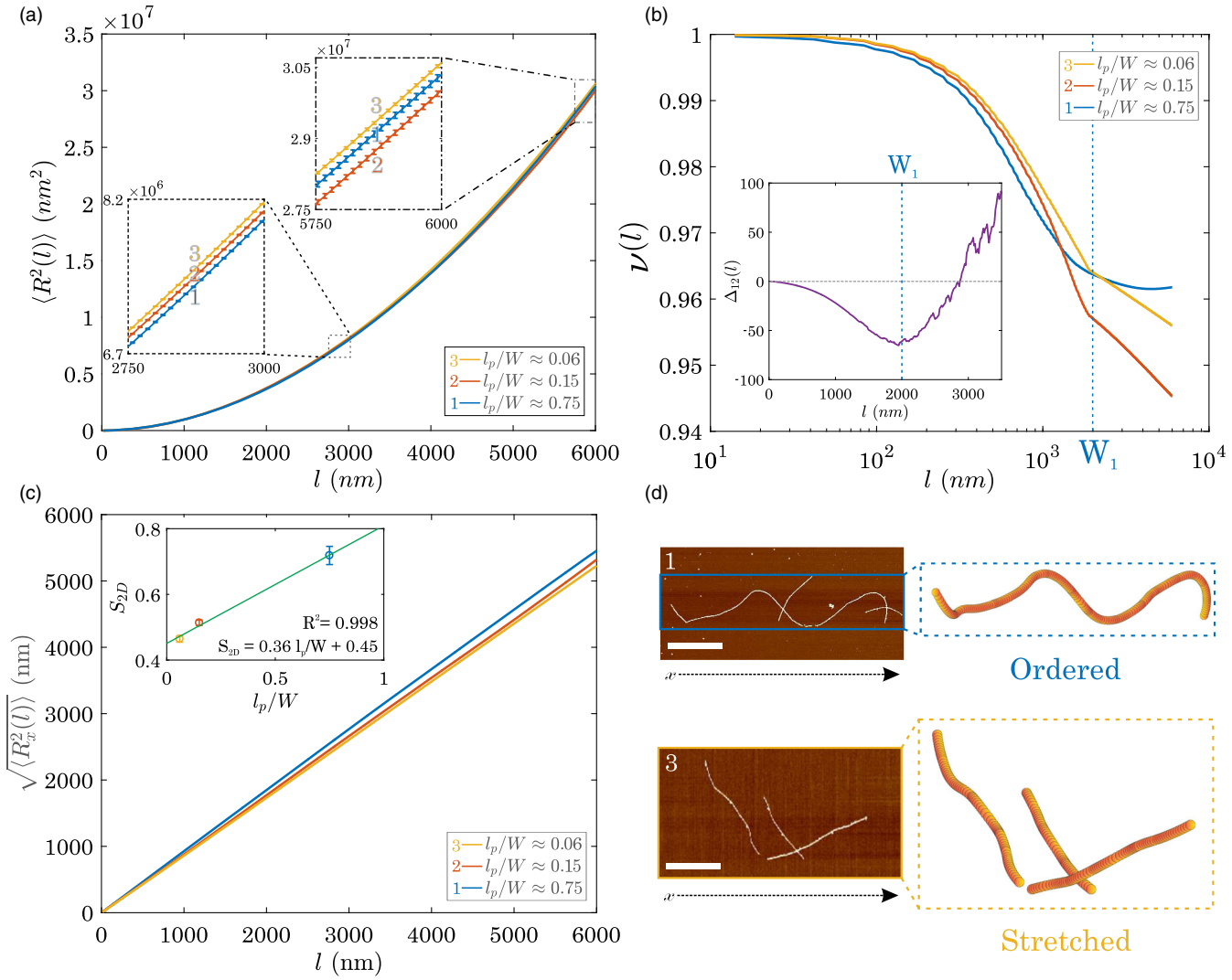

FIG. 2. Statistics of amyloid fibrils in slits of various widths (10 s of plasma treatment), characterized by the ratio l_p/W, with a number of fibrils of $n_{f,1} = 1061$, $n_{f,2} = 1482$, and $n_{f,3} = 3493$, individual segment statistics in Fig. S7 [29]. (a) End-to-end distance of fibrils $\langle R^2(l)\rangle$ as a function of internal contour length l. Inset, bottom left: Enlargement of the $\langle R^2(l)\rangle$ at small l. Inset, top right: Enlargement of $\langle R^2(l)\rangle$ for higher l. (b) Decay of scaling exponent $\nu(l)$ as a function of l. Dashed blue line at $W_1 = 2000$ nm. Inset: Δ_{12}, difference in the slopes of $\langle R^2(l)\rangle_{1,2}$. (c) $\sqrt{\langle R_x^2(l)\rangle}$, with x the direction of the slit. Inset: Order parameter S_{2D} as a function of the confinement l_p/W with linear fit and corresponding fitting parameters. (d) AFM images (left) and schematics (right) of amyloid fibrils in the extreme cases of slits "1" (top) and "3" (bottom). Scale bar is 2 μm.

(see Fig. S8 of SM [29]). However, as Δ_{12} is the difference in the slopes, the linear trend is canceled out and the higher orders become the trend-dominating terms. At $l = 2000$ nm, corresponding to W_1, a minimum is reached, at which point the confinement takes over and Δ_{12} starts to increase, eventually becoming positive. Thus, the confinement begins to rule as soon as the width of the slit and the contour length have the same dimension. At this length scale, we again expect $\langle R(l)^2\rangle \approx c_W l^2$, this time due to the confinement [16]. However, in this case the prefactor c_W depends on W, so that the linear terms in Δ_{12} do not cancel out, leading to the quasilinear increase observed in Fig. 2(b). We note that taking into account these considerations, an alternative representation of Fig. 2(a) (see Fig. S8 [29]) is possible, where thanks to the scaling behavior $\langle R(l)^2\rangle \sim l^2$, the crossover between the curves "1" and "2" can be highlighted by plotting $\langle R^2(l)\rangle - l^2$ as a function of l.

The decay of the scaling exponent [Fig. 2(b)] brings further evidence to support the observed change in regime. Indeed, at $l \ll W_1$ the trend of the decays follows that of the force; the fibrils experiencing the highest force decay the slowest away from $\nu = 1$, the exponent of a rigid rod [34]. However, the behavior of $\nu_1(l)$ clearly demonstrates the effect of the confinement. Its decay slows down earlier than that of the other two and reaches a plateau at $l \approx W_1$.

The plateau reaches a value of $\nu_1 \approx 0.96$, which is far from either the 2D or 3D excluded-volume exponents, $\nu_{2D} = 0.75$ and $\nu_{3D} \approx 0.588$, that are the asymptotic values usually reached at large length scales [34,35]. In other words, the fibrils are too short to reach self-similar behavior and they remain close to the rod regime. The other two curves, on the other hand, continue to decay according to the strength of the force. By $l = W$, ν_1 has taken over ν_2 already, in agreement with the behavior shown in the inset; furthermore, and most remarkably, at $l \gg W$, ν_1 has even taken over ν_3, demonstrating that confinement not only competes with the force but even dominates.

Both confinement and a pulling force are known to independently create alignment [6,8,13,14,16,36]. The quantities reported so far do not provide any information on the fibril orientation. Therefore, to assess this feature within the present system, where both effects act simultaneously, we plotted the $\sqrt{\langle R_x^2(l)\rangle}$ as a function of l, with x the direction of the slit [in Fig. 2(c)]. This construct enables the distinction of the dominant mechanism determining the alignment of fibrils. Indeed, a linear dependence is expected in all cases, $\sqrt{\langle R_x^2(l)\rangle} \approx d_W l$, as confirmed by Fig. 2(c). Nevertheless, the slope d_W changes according to the specific slit considered. We observe that the ranking 3-2-1 holds at all length scales, thus demonstrating that confinement is always driving the orientation of fibrils. This is in contrast with the results in Figs. 2(a) and 2(b), where the force was the driving mechanism at small length scales. To further validate and quantify this observation, we considered the order parameter $S_{2D} = 2\langle \cos^2 \phi_s \rangle - 1$ [33], where ϕ_s is the angle formed by the director of the slit and the vector tangent to the fibril at the curvilinear coordinate s. The average is computed from the orientation distribution of the fibrils (Fig. S10 [29]). For polymers perfectly aligned along the slit $S_{2D} = 1$, while $S_{2D} = 0$ denotes a random orientation. The inset in Fig. 2(c) shows that S_{2D} is an increasing function of l_p/W, displaying an approximately linear behavior, as was previously observed for other biopolymers under confinement [21]. We note that the linear fit has a nonzero intercept. This is due to the fact that the force cannot be decoupled from the confinement, therefore shifting the intercept away from zero for an infinite slit. The positive slope of this dependence, however, confirms that for this system alignment is determined by confinement, despite the higher degree of stretched fibrils in the wider slits induced by a stronger pulling force.

Indeed, under closer inspection of the AFM images of the various capillaries, Fig. 2(d), we note that the fibrils in slit "1" are more relaxed than those in slit "3," which are highly stretched, as expected from Fig. 2(a). However, in slit "3" there is also a significant amount of fibrils oriented perpendicularly to the main axis, which lowers the value of S_{2D} and thus resolves the apparent contradiction suggested by the negative correlation between the alignment and the stretching of fibrils.

In order to further confirm our interpretation of the results, we carried out coarse-grained simulations using LAMMPS [37]. The full details of the implementation can be found in Sec. S1.5 of SM [29]. In short, we considered a collection of polymers in two dimensions characterized by bending rigidity and excluded-volume interactions, and confined between two walls separated by a distance W. The capillary force was mimicked by pulling the two ends of each polymer along the direction of the slit with a force proportional to W, as dictated by Eq. (1). However, besides the correct scaling with W, the exact prefactor g of the force was left as a free parameter able to scan a broad range of forces. We note that a model system, where W, l_p, and contour length l_0 were scaled down by a factor of 10, was considered for computational purposes. The size of the monomers, however, was maintained, thus influencing the excluded-volume interactions.

For a suitable choice of g, the simulations qualitatively reproduce the main features of the experimental results (Fig. 3). Indeed, force- and confinement-dominated regimes for $\langle R^2(l)\rangle$ are observed at low and large length scales, respectively, as indicated by the rankings $1'$-$2'$-$3'$ and $2'$-$1'$-$3'$ of the curves. In contrast, the order parameter S_{2D} is determined by the confinement for all slits, with an approximately linear dependence on l_p/W. Remarkably, this feature can be tuned by changing the prefactor g

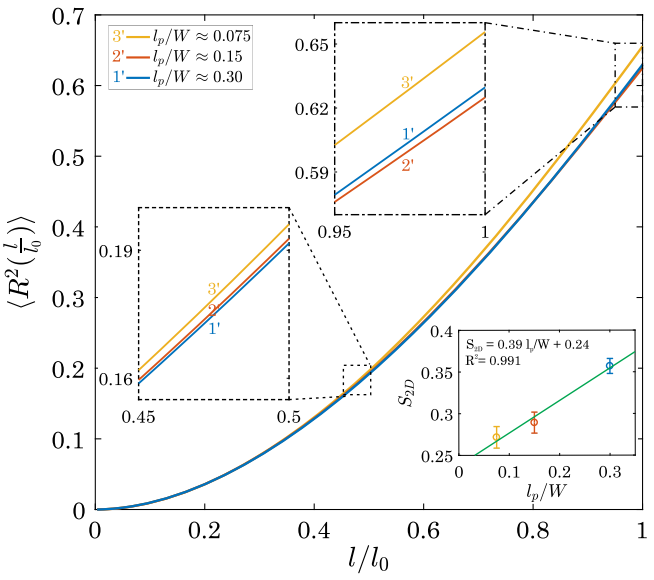

FIG. 3. Simulated $\langle R^2(l/l_0)\rangle$ as a function of l/l_0, where l_0 is the total contour length of the simulated chains, in different degrees of confinement l_p/W. The capillary force follows the relation $f = 10^{-3}(1.2W/l_p + 1)$. Inset, middle left: Enlargement of the $\langle R^2(l/l_0)\rangle$ at low l/l_0, relative position of the curves is $1'$-$2'$-$3'$. Inset, top right: Enlargement of the $\langle R^2(l/l_0)\rangle$ at high l/l_0, trend becomes $2'$-$1'$-$3'$. Inset, bottom right: Order parameter S_{2D} as a function of the degree of confinement l_p/W. Linear fit and its fitting parameters are reported in the top left-hand corner.

(see Fig. S12 [29]). Indeed, larger capillary forces lead to a nonmonotonic behavior of S_{2D}, indicating that the force drives the alignment at low values of l_p/W, while confinement plays the leading role at larger l_p/W (see Sec. S3.2 of SM [29]). The impact of strong pulling forces on alignment reported in the simulations is in line with the experimental observations made for larger plasma times, where the average orientation of fibrils was indeed affected (see Fig. S5 [29]).

In conclusion, we have addressed the fine interplay between a pulling force and spatial confinement simultaneously acting on amyloid fibrils. Depending on the length scale, the extension of a fibril was force dominated (at short length scales) or confinement dominated (at large length scales). In contrast, the alignment of fibrils was found to be confinement dominated at all length scales. Complementary simulations qualitatively corroborated the experimental results and further revealed a variety of possible regimes controlled by the strength of the capillary force. Our results not only highlight this subtle interplay but also may potentially guide our understanding of significant *in vivo* amyloid phenomena in blood vessels, thus shedding light on the progression of amyloid-related diseases. More in general, these results bear a general significance to all classes of semiflexible biopolymers subjected to high strains and confinement, well beyond the exclusive case of amyloids. For instance, DNA in both eukaryotes [38] and bacteria [39,40] is spatially confined and strained during transcription by polymerase [41] or during cell division mitosis [42–44]. In muscles, actin and myosin fibers are both constrained and undergo constant stress [45]; the same can be said of collagen [46], and of cellulose in the cell wall [47].

The authors wish to acknowledge Dr. G. Nyström and Dr. S. Bolisetty for their scientific discussions, Paride Azzari for his insightful discussions, Dr. Sergii Pud for his assistance in the fabrication of the microchannel templates, Professor Peter Fischer for the use of the plasma cleaner, Peter Biegler for his assistance in maintaining the said plasma cleaner, Dr. Tobias Schwarz for the light microscopy images, and Robert Axelrod for proofreading. A. J. acknowledges support by the Swiss National Science Foundation (Grants No. P2ELP2_168554 and No. P300P2_177768).

*raffaele.mezzenga@hest.ethz.ch
†Present address: Departamento de Física Teórica de la Materia Condensada, Universidad Autónoma de Madrid, Madrid, Spain.

[1] C. M. Dobson, Protein misfolding, evolution and disease, Trends Biochem. Sci. **24**, 329 (1999).
[2] D. J. Selkoe, Folding proteins in fatal ways, Nature (London) **426**, 900 (2003).
[3] F. Chiti and C. M. Dobson, Protein misfolding, functional amyloid, and human disease, Annu. Rev. Biochem. **75**, 333 (2006).
[4] D. M. Fowler, A. V. Koulov, W. E. Balch, and J. W. Kelly, Functional amyloid from bacteria to humans, Trends Biochem. Sci. **32**, 217 (2007).
[5] M. W. Mosesson, Fibrinogen heterogeneity, Ann. N.Y. Acad. Sci. **408**, 97 (1983).
[6] V. Castelletto and I. W. Hamley, β-Lactoglobulin fibers under capillary flow, Biomacromolecules **8**, 77 (2006).
[7] E. K. Hill, B. Krebs, D. G. Goodall, G. J. Howlett, and D. E. Dunstan, Shear flow induces amyloid fibril formation, Biomacromolecules **7**, 10 (2006).
[8] R. Adachi, K. I. Yamaguchi, H. Yagi, K. Sakurai, H. Naiki, and Y. Goto, Flow-induced alignment of amyloid protofilaments revealed by linear dichroism, J. Biol. Chem. **282**, 8978 (2007).
[9] C. N. Trumbore, Shear-induced amyloid formation in the brain: I. Potential vascular and parenchymal processes, J. Alzheimer's Dis. **54**, 457 (2016).
[10] S. Mankar, A. Anoop, S. Sen, and S. K. Maji, Nanomaterials: Amyloids reflect their brighter side, Nano Rev. **2**, 1 (2011).
[11] G. Nyström, M. P. Fernández-Ronco, S. Bolisetty, M. Mazzotti, and R. Mezzenga, Amyloid templated gold aerogels, Adv. Mater. **28**, 472 (2016).
[12] F. G. Pearce, S. H. Mackintosh, and J. a. Gerrard, Formation of amyloid-like fibrils by ovalbumin and related proteins under conditions relevant to food processing, J. Agric. Food Chem. **55**, 318 (2007).
[13] P. de Gennes, *Scaling Concepts in Polymer Physics* (Cornell University Press, Ithaca, 1979).
[14] J. F. Marko and E. D. Siggia, Stretching DNA, Macromolecules **28**, 8759 (1995).
[15] C. Bustamante, Z. Bryant, and S. B. Smith, Ten years of tension: Single-molecule DNA mechanics, Nature (London) **421**, 423 (2003).
[16] T. Odijk, On the statistics and dynamics of confined or entangled stiff polymers, Macromolecules **16**, 1340 (1983).
[17] T. T. Perkins, D. E. Smith, R. G. Larson, and S. Chu, Stretching of a single tethered polymer in a uniform flow, Science **268**, 83 (1995).
[18] T. T. Perkins, D. E. Smith, and S. Chu, Single polymer dynamics in an elongational flow, Science **276**, 2016 (1997).
[19] X. R. Bao, H. J. Lee, and S. R. Quake, Behavior of Complex Knots in Single DNA Molecules, Phys. Rev. Lett. **91**, 265506 (2003).
[20] A. Japaridze, E. Orlandini, K. B. Smith, L. Gmür, F. Valle, C. Micheletti, and G. Dietler, Spatial confinement induces hairpins in nicked circular DNA, Nucleic Acids Res. **45**, 4905 (2017).
[21] K. B. Smith, J.-N. Tisserant, S. Assenza, M. Arcari, G. Nyström, and R. Mezzenga, Confinement-induced ordering and self-folding of cellulose nanofibrils, Adv. Sci. **6**, 1801540 (2019).
[22] G.-L. He, R. Messina, H. Löwen, A. Kiriy, V. Bocharova, and M. Stamm, Shear-induced stretching of adsorbed polymer chains, Soft Matter **5**, 3014 (2009).

[23] R. Li and J. Wang, Stretching a semiflexible polymer in a tube, Polymers **8**, 328 (2016).
[24] J. Wang and K. Li, Statistical behaviors of semiflexible polymer chains stretched in rectangular tubes, Polymers **11**, 260 (2019).
[25] J. M. Jung, G. Savin, M. Pouzot, C. Schmitt, and R. Mezzenga, Structure of heat-induced β-lactoglobulin aggregates and their complexes with sodium-dodecyl sulfate, Biomacromolecules **9**, 2477 (2008).
[26] J. Adamcik, J.-M. Jung, J. Flakowski, P. De Los Rios, G. Dietler, and R. Mezzenga, Understanding amyloid aggregation by statistical analysis of atomic force microscopy images, Nat. Nanotechnol. **5**, 423 (2010).
[27] S. Jordens, J. Adamcik, I. Amar-Yuli, and R. Mezzenga, Disassembly and reassembly of amyloid fibrils in water-ethanol mixtures, Biomacromolecules **12**, 187 (2011).
[28] J. Adamcik and R. Mezzenga, Proteins fibrils from a polymer physics perspective, Macromolecules **45**, 1137 (2012).
[29] See Supplemental Material at http://link.aps.org/supplemental/10.1103/PhysRevLett.124.118102 for a full account on the materials and methods in Sec. S1, which includes Ref. [30].
[30] F. Wu, B. G. C. van Schie, J. E. Keymer, and C. Dekker, Symmetry and scale orient Min protein patterns in shaped bacterial sculptures, Nat. Nanotechnol. **10**, 719 (2015).
[31] F. F. Ouali, G. McHale, H. Javed, C. Trabi, N. J. Shirtcliffe, and M. I. Newton, Wetting considerations in capillary rise and imbibition in closed square tubes and open rectangular cross-section channels, Microfluidics Nanofluidics **15**, 309 (2013).
[32] P. M. Triolo and J. D. Andrade, Surface modification and evaluation of some commonly used catheter materials. I. Surface properties, J. Biomed. Mater. Res. **17**, 129 (1983).
[33] I. Usov and R. Mezzenga, FiberApp: An open-source software for tracking and analyzing polymers, filaments, biomacromolecules, and fibrous objects, Macromolecules **48**, 1269 (2015).
[34] F. Valle, M. Favre, P. De Los Rios, A. Rosa, and G. Dietler, Scaling Exponents and Probability Distributions of DNA End-to-End Distance, Phys. Rev. Lett. **95**, 158105 (2005).
[35] C. Lara, I. Usov, J. Adamcik, and R. Mezzenga, Sub-Persistence-Length Complex Scaling Behavior in Lysozyme Amyloid Fibrils, Phys. Rev. Lett. **107**, 238101 (2011).
[36] A. S. Sassi, S. Assenza, and P. De Los Rios, Shape of a Stretched Polymer, Phys. Rev. Lett. **119**, 037801 (2017).
[37] S. Plimpton, Fast parallel algorithms for short-range molecular dynamics, J. Comput. Phys. **117**, 1 (1995).
[38] B. Alberts, A. Johnson, J. Lewis, M. Raff, K. Roberts, and P. Walter, in *Molecular Biology of the Cell*, 4th ed. (Garland Science, New York, 2002), pp. 191–234.
[39] D. J. Sherratt, Bacterial chromosome dynamics, Science **301**, 780 (2003).
[40] F. Wu, A. Japaridze, X. Zheng, J. Wiktor, J. W. J. Kerssemakers, and C. Dekker, Direct imaging of the circular chromosome in a live bacterium, Nat. Commun. **10**, 2194 (2019).
[41] R. K. Saiki, D. H. Gelfand, S. Stoffel, S. J. Scharf, R. Higuchi, G. T. Horn, K. B. Mullis, and H. A. Erlich, Primer-directed enzymatic amplification of DNA with a thermostable DNA polymerase, Science **239**, 487 (1988).
[42] S. P. Bell and A. Dutta, DNA replication in eukaryotic cells, Annu. Rev. Biochem. **71**, 333 (2002).
[43] M. Meselson and F. W. Stahl, The replication of DNA in Escherichia coli, Proc. Natl. Acad. Sci. U.S.A. **44**, 671 (1958).
[44] K. S. Bloom, Beyond the code: The mechanical properties of DNA as they relate to mitosis, Chromosoma **117**, 103 (2008).
[45] T. D. Pollard, R. R. Weihing, and M. R. Adelman, Actin and myosin and cell movement, CRC Crit. Rev. Biochem. **2**, 1 (1974).
[46] K. E. Kadler, D. F. Holmes, J. A. Trotter, and J. A. Chapman, Collagen fibril formation, Biochem. J. **316**, 1 (1996).
[47] C. Somerville, S. Bauer, G. Brininstool, M. Facette, T. Hamann, J. Milne, E. Osborne, A. Paredez, S. Persson, T. Raab, S. Vorwerk, and H. Youngs, Toward a systems approach to understanding plant cell walls, Science **306**, 2206 (2004).